Dark quantum imaging with fermions

Shu Gan,[1] De-Zhong Cao,[2] and Kaige Wang[1,*]
[1]*Department of Physics, Applied Optics Beijing Area Major Laboratory, Beijing Normal University, Beijing 100875, China*
[2]*Department of Physics, Yantai University, Yantai 264005, China*
(Received 6 May 2009; published 12 October 2009)

Quantum imaging with a thermal source of fermions is analyzed and compared with that of bosons. Due to the Pauli exclusive principle and Fermi-Dirac statistics, fermions can manifest antibunching effects in the second-order correlation function. Our analysis finds that quantum imaging with free fermions can construct dark patterns against a bright intensity background. This distinguishing feature highlights the quantum nature of fermions without any classical analog. A scheme of magnifying ghost imaging of an electron microscope is also proposed.

DOI: 10.1103/PhysRevA.80.043809 PACS number(s): 42.50.St, 42.50.Ar, 42.50.Dv, 42.30.Va

I. INTRODUCTION

Quantum imaging has drawn much attention in recent years [1]. Contrary to conventional optical imaging and interference using coherent light, the quantum image is visible in spatial intensity correlation measurement but not in the intensities themselves. In the early studies, the schemes of quantum imaging, such as "ghost" imaging, ghost interference and subwavelength lithography, were proposed by using an entangled two-photon source generated by spontaneous parametric downconversion [2–5]. These effects were regarded as the evidence of quantum entanglement and nonlocality. However, the understanding was challenged by the later discoveries [6–10] that a thermal light source can play a role similar to that of the entangled two-photon source in those quantum imaging schemes. These effects can be explained by the spatial intensity correlation of the thermal light source, which has been known since Hanbury-Brown and Twiss (HBT) proposed a technique of intensity interferometry for measuring the angular sizes of visual stars [11]. Far beyond the astronomical application, the HBT effect involves fundamental arguments regarding, for example, classical vs quantum interpretation, and one-photon vs two-photon interference, etc. and some of them is even revived in the recent debate [12,13]. The HBT effect reflects the nature of the high-order field correlation, either classical or quantum field. The physics behind is that each point of a spatially incoherent source produces coherence of the field at two separate positions, after having traveled different paths, and the coherent information can be acquired through the intensity correlation measurement.

Since quantum mechanics was established, investigations on interference and imaging have been extended from photon source to massive particle sources. In 1961 an actual double-slit experiment with electrons was first performed by Jönsson [14]. Since the interference of particles is governed by quantum field, the experiment opened a gateway to fundamental tests of quantum mechanics. The extension also found wide and powerful applications in electron microscopy and electron holography. It is noteworthy that, in the first-order interference and imaging observed by the intensity measurement (i.e., one-particle detection), the quantum fields of bosons and fermions follow the same principle and thus their basic phenomena behave the same. As for the high-order correlation of the quantum fields, however, the quantum interference in HBT effect shows bunching for bosons and antibunching for fermions and has been demonstrated in the experimental observations [15–19]. The bunching and antibunching effects manifest the nature of quantum statistics associated with exchange symmetry of wave function for identical particles.

In this paper, we study quantum imaging in the intensity correlation observation by using a thermal fermion source. This extension is not trivial since, unlike the optical version, the correlation of fermions concerns quantum nature without any classical analog. Quantum imaging with fermions differs from quantum imaging with bosons in that a dark image for fermions while a bright one for bosons. The dark quantum imaging may increase the visibility of the interference pattern up to unit, which is not possible for thermal bosons. Moreover, since the sources of massive particles are not coherent, the interference and imaging technique without the requirement of spatial coherence may be practically useful, such as for electron microscopy and holography. The paper is organized as follows. In Sec. II, we recast the first- and second-order correlation functions of multimode quantum mixed state for both bosons and fermions. In Secs. III and IV, the subwavelength interference and ghost imaging of fermions are discussed, respectively. An application of ghost imaging to electron microscope is proposed in Sec. V.

II. FIRST- AND SECOND-ORDER CORRELATION FUNCTIONS OF MULTIMODE QUANTUM MIXED STATES

We consider quasimonochromatic, noninteracting, nonrelativistic, and polarized particles. It has been shown that for both bosons [20] and fermions [21], the correlation functions of partially polarized or totally unpolarized particles can be described by the correlation functions of polarized particles and the degree of polarization. The quantum correlation functions of fermions were theoretically discussed by Silver-

*Author to whom correspondence should be addressed. wangkg@bnu.edu.cn

man [22] and Tyc [23] who assumed a mixture of number states with a Poissonian distribution of the particle numbers where each particle has the same momentum distribution. Here we recast the first- and second-order correlation functions by considering a general multimode mixed state designated by $\rho=\Pi_{\mathbf{k}}\rho_{\mathbf{k}}$, where the density operator for the mode with wave vector $\mathbf{k}$ is assumed to be diagonal $\rho_{\mathbf{k}}=\Sigma_{n_{\mathbf{k}}}P_{\mathbf{k}}(n_{\mathbf{k}})|n_{\mathbf{k}}\rangle\langle n_{\mathbf{k}}|$, with $\Sigma_{n_{\mathbf{k}}}\rightarrow\Sigma_{n_{\mathbf{k}}=0}^{\infty}$ for bosons and $\Sigma_{n_{\mathbf{k}}}\rightarrow\Sigma_{n_{\mathbf{k}}=0}^{1}$ for fermions due to the Pauli exclusion principle. $P_{\mathbf{k}}(n_{\mathbf{k}})$ is the particle number distribution for mode $\mathbf{k}$. We express the mixed state as

$$\rho=\prod_{\mathbf{k}}\rho_{\mathbf{k}}=\prod_{\mathbf{k}}\sum_{n_{\mathbf{k}}}P_{\mathbf{k}}(n_{\mathbf{k}})|n_{\mathbf{k}}\rangle\langle n_{\mathbf{k}}|$$
$$=\sum_{n_{\mathbf{k}_1}}\sum_{n_{\mathbf{k}_2}}\cdots P_{\mathbf{k}_1}(n_{\mathbf{k}_1})P_{\mathbf{k}_2}(n_{\mathbf{k}_2})\cdots|n_{\mathbf{k}_1},n_{\mathbf{k}_2}\cdots\rangle\langle n_{\mathbf{k}_1},n_{\mathbf{k}_2}\cdots|. \tag{1}$$

Let $a_{\mathbf{k}}$ and $a_{\mathbf{k}}^{\dagger}$ be the annihilation and creation operators of occupation number for mode $\mathbf{k}$, respectively, the commutation relations are written as

$$[a_{\mathbf{k}},a_{\mathbf{k}'}]_{\mp}=0,\quad [a_{\mathbf{k}}^{\dagger},a_{\mathbf{k}'}^{\dagger}]_{\mp}=0,\quad [a_{\mathbf{k}},a_{\mathbf{k}'}^{\dagger}]_{\mp}=\delta_{\mathbf{k}\mathbf{k}'}, \tag{2}$$

where the commutation relation $[\ ]_-$ and the anticommutation relation $[\ ]_+$ are referred to bosons and fermions, respectively. Using Eq. (2), we arrive at the first-order correlation function for state (1)

$$\langle a_{\mathbf{k}}^{\dagger}a_{\mathbf{k}'}\rangle=\mathrm{Tr}(\rho a_{\mathbf{k}}^{\dagger}a_{\mathbf{k}'})=\delta_{\mathbf{k}\mathbf{k}'}\langle n_{\mathbf{k}}\rangle, \tag{3}$$

where the average occupation number $\langle n_{\mathbf{k}}\rangle=\Sigma_{n_{\mathbf{k}}}n_{\mathbf{k}}P_{\mathbf{k}}(n_{\mathbf{k}})$ describes the power spectrum of the particle source. The first-order correlation function (3) has the same form for both bosons and fermions so that they show the same phenomena in the first-order interference.

Since each mode of fermions has only two occupations, 0 and 1, the number distribution is given by $P_{\mathbf{k}}(n_{\mathbf{k}})=\langle n_{\mathbf{k}}\rangle^{n_{\mathbf{k}}}/(1-\langle n_{\mathbf{k}}\rangle)^{n_{\mathbf{k}}-1}$. However, bosons are assumed to be in the thermal equilibrium, and $P_{\mathbf{k}}(n_{\mathbf{k}})$ satisfies the Bose-Einstein distribution, $P_{\mathbf{k}}(n_{\mathbf{k}})=\langle n_{\mathbf{k}}\rangle^{n_{\mathbf{k}}}/(1+\langle n_{\mathbf{k}}\rangle)^{n_{\mathbf{k}}+1}$. The second-order correlation function is thus obtained as

$$\langle a_{\mathbf{k}}^{\dagger}a_{\mathbf{k}'}^{\dagger}a_{\mathbf{k}''}a_{\mathbf{k}'''}\rangle=\langle a_{\mathbf{k}}^{\dagger}a_{\mathbf{k}'''}\rangle\langle a_{\mathbf{k}'}^{\dagger}a_{\mathbf{k}''}\rangle\pm\langle a_{\mathbf{k}}^{\dagger}a_{\mathbf{k}''}\rangle\langle a_{\mathbf{k}'}^{\dagger}a_{\mathbf{k}'''}\rangle, \tag{4}$$

where the positive and negative signs imply the bunching effect for bosons and antibunching effect for fermions, respectively.

We now consider a quantum field traveling along z axis. In the paraxial approximation the field operator is described as $\psi(x,z,t)=\psi(x)\exp[i(kz-\omega_k t)]$ with $\psi(x)=(1/\sqrt{2\pi})\int a(q)\exp(iqx)dq$, where k and ω_k are the carrier wave number and frequency, respectively. For simplicity, one-dimensional transverse wave number q and position x are considered. Similar to a linear optical system, the transmission of quantum field is given by

$$\phi(x)=\int h(x,x')\psi(x')dx'=\int\tilde{h}(x,-q)a(q)dq, \tag{5}$$

where $\psi(x)$ and $\phi(x)$ are the source and output fields, respectively; $h(x,x')$ is the impulse response function and $\tilde{h}(x,q)=(1/\sqrt{2\pi})\int h(x,x')\exp(-iqx')dx'$. When the source is assumed in the multimode state (1) with transverse mode index q, Eqs. (3) and (4) are fulfilled with q replacing $\mathbf{k}$. Using Eqs. (3)–(5), the first-order and second-order spatial correlation functions of outgoing quantum field $\phi(x)$ can be obtained to be

$$G^{(1)}(x_1,x_2)=\langle\phi^{\dagger}(x_1)\phi(x_2)\rangle$$
$$=\int\langle n_q\rangle\tilde{h}^{*}(x_1,-q)\tilde{h}(x_2,-q)dq, \tag{6a}$$

$$G^{(2)}(x_1,x_2)=\langle\phi^{\dagger}(x_1)\phi^{\dagger}(x_2)\phi(x_2)\phi(x_1)\rangle$$
$$=G^{(1)}(x_1,x_1)G^{(1)}(x_2,x_2)\pm|G^{(1)}(x_1,x_2)|^2. \tag{6b}$$

In ghost imaging, however, the particles flux is divided into two by a beamsplitter, each of which travels in individual path characterized by the impulse response function $h_j(x,x')(j=1,2)$. Then the cross correlation functions are written as

$$G_{ij}^{(1)}(x_1,x_2)=\langle\phi_i^{\dagger}(x_1)\phi_j(x_2)\rangle$$
$$=\int\langle n_q\rangle\tilde{h}_i^{*}(x_1,-q)\tilde{h}_j(x_2,-q)dq,$$
$$(i=1,2;j=1,2), \tag{7a}$$

$$G_{12}^{(2)}(x_1,x_2)=\langle\phi_1^{\dagger}(x_1)\phi_2^{\dagger}(x_2)\phi_2(x_2)\phi_1(x_1)\rangle$$
$$=G_{11}^{(1)}(x_1,x_1)G_{22}^{(1)}(x_2,x_2)\pm|G_{12}^{(1)}(x_1,x_2)|^2. \tag{7b}$$

III. DARK SUBWAVELENGTH INTERFERENCE FRINGE

Wang and Cao [9] first proposed that when a double slit was illuminated by a multimode thermal light field, the interference fringe is not visible in the intensity observation but can be extracted through the spatial intensity correlation measurement. Similar to an entangled two-photon source, the fringe exhibits the subwavelength feature. The proposal was soon demonstrated in the experiments [24,25]. Here we reconsider this effect by comparing a fermion source with the boson one.

In the scheme of double-slit interference, a double slit, described by the transmission function $D(x)=\mathrm{rect}[(x-d/2)/b]+\mathrm{rect}[(x+d/2)/b]$ with slit width b and slit distance d, is placed at distance z_0 from the source and distance z from the detection screen. In the far-field limit, the impulse response function of the scheme is approximately given by

$$\tilde{h}_D(x,-q) = \sqrt{\frac{k}{2\pi i z}} \times \exp\left[i\left(kz_0 + kz - \frac{z_0 q^2}{2k} + \frac{kx^2}{2z} \right) \right] \tilde{D}\left(\frac{kx}{z} - q \right), \tag{8}$$

where $\tilde{D}(q)=(2b/\sqrt{2\pi})\mathrm{sinc}(qb/2)\cos(qd/2)$ is the Fourier transform of the double-slit function $D(x)$. Substituting Eq. (8) into Eq. (6a) we obtain

$$G^{(1)}(x_1,x_2) = \frac{k}{2\pi z}\int \langle n_q\rangle \tilde{D}^*\left(\frac{kx_1}{z} - q \right)\tilde{D}\left(\frac{kx_2}{z} - q \right)dq. \tag{9}$$

$G^{(1)}(x,x)$ describes first-order or one-particle double-slit interference for both bosons and fermions. To be specific, we assume a Gaussian spectrum for the source

$$\langle n_q\rangle = \frac{\langle n\rangle}{\sqrt{2\pi w}}\exp\left(-\frac{q^2}{2w^2} \right), \tag{10}$$

where w and $\langle n\rangle=\int\langle n_q\rangle dq$ are the spectral bandwidth and the mean particle number of the source, respectively. In the narrow bandwidth limit, $\langle n_q\rangle \to \langle n\rangle \delta(q)$, Eq. (9) has the analytical form

$$G^{(1)}(x_1,x_2) = \frac{k\langle n\rangle}{2\pi z}\tilde{D}^*\left(\frac{kx_1}{z} \right)\tilde{D}\left(\frac{kx_2}{z} \right), \tag{11}$$

which implies the first-order coherence. $G^{(1)}(x,x) \propto |\tilde{D}(kx/z)|^2$ describes perfect interference fringe. Therefore the quantum mixed state (1) with a narrow bandwidth possesses good spatial coherence and can carry out the first-order interference with a high visibility. It is noticeable that in terms of the first-order interference there is no difference between bosons and fermions. In the broad bandwidth limit, however, $\langle n_q\rangle \to \langle n\rangle / w$, Eq. (9) becomes

$$G^{(1)}(x_1,x_2) = \frac{k\langle n\rangle}{\sqrt{2\pi z w}}\tilde{D}\left[\frac{k}{z}(x_2 - x_1) \right]. \tag{12}$$

The first-order interference disappears owing to $G^{(1)}(x,x) \propto \tilde{D}(0)$. Physically, the degradation of the first-order interference can be explained by the fact that the multimode quantum field illuminating the double slit propagates in various directions. Nevertheless, Eq. (12) implicates that the information of interference has not been destroyed but preserved in the spatial correlation of two positions, which is unable to be observed in one-particle detection.

Two-particle correlation measurement in the observation plane is proportional to $\langle \phi^\dagger(x_1)\phi(x_1)\phi^\dagger(x_2)\phi(x_2)\rangle$. When $x_1 \neq x_2$, the second-order correlation function $G^{(2)}(x_1,x_2) \equiv \langle \phi^\dagger(x_1)\phi^\dagger(x_2)\phi(x_2)\phi(x_1)\rangle = \langle \phi^\dagger(x_1)\phi(x_1)\phi^\dagger(x_2)\phi(x_2)\rangle$ is valid for both bosons and fermions. However, $G^{(2)}(x,x)$ describes a two-particle absorption intensity distribution for bosons while $G^{(2)}(x,x)=0$ for any quantum state of fermions due to the Pauli exclusion principle. We have demonstrated that the second-order correlation Eq. (6b) is hold for state (1). Therefore, coherence information contained in the first-order correlation function $G^{(1)}(x_1,x_2)$ can be extracted through the two-particle correlation measurement.

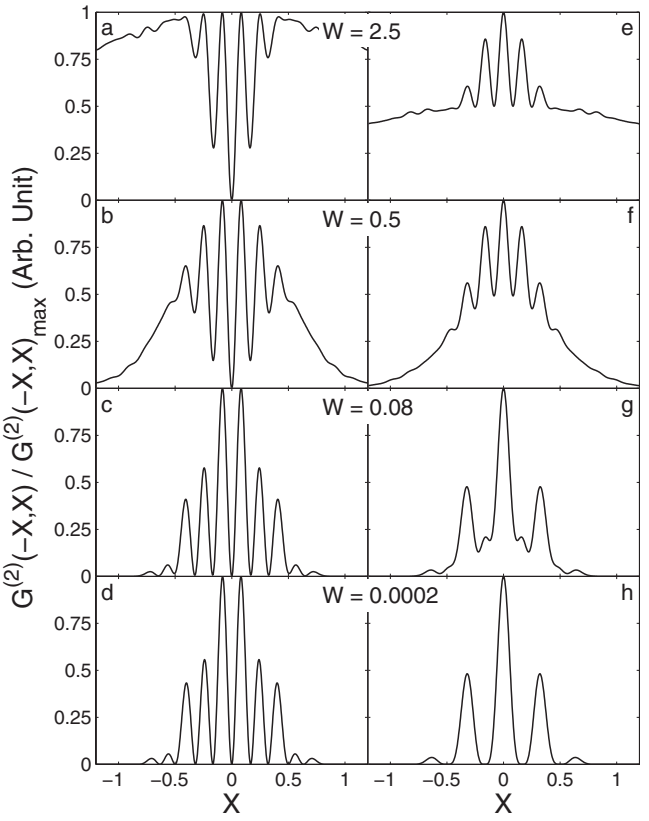

FIG. 1. Subwavelength interference patterns of a double-slit illuminated by a thermal fermion source in (a)–(d) and a boson source in (e)–(h). The multimode thermal source has the Gaussian spectral distributions with different normalized bandwidth $W=wb/(2\pi)$. $X=xkb/(2\pi z)$ is the normalized position in the detection plane, and the double-slit parameters are taken to be $b=d/3$.

For simplicity, we focus on the correlation between a pair of symmetric positions, $-x$ and x. In the broad bandwidth limit we obtain

$$G^{(2)}(-x,x) \propto \tilde{D}^2(0) \pm \tilde{D}^2(2kx/z) \propto 1 \pm \mathrm{sinc}^2\left(\frac{b}{2}\frac{2kx}{z} \right)\cos^2\left(\frac{d}{2}\frac{2kx}{z} \right). \tag{13}$$

Equation (13) shows that the two-particle interference for the incoherent fermion source reveals a dark and inverted fringe in the bright background with perfect visibility 100%, whereas for thermal bosons, as we have known, it displays a bright fringe with the maximum visibility 33.3% [9]. Both of them exhibit subwavelength feature: the spacing of fringes is the half of that for the first-order interference.

For the source with the spectral distribution [Eq. (10)], using Eqs. (6), (8), and (9), we calculate the second-order correlation function $G^{(2)}(-X,X)$ of the normalized transverse position $X=xkb/(2\pi z)$. Figure 1 shows the two-particle interference patterns of fermions (left column) and bosons (right column) for different spectral bandwidths. When the normalized bandwidth is large, i.e., $W \equiv wb/2\pi = 2.5$, the interference fringe of the fermions [Fig. 1(a)] is a "dark" one. This phenomenon is particularly interesting since it implies

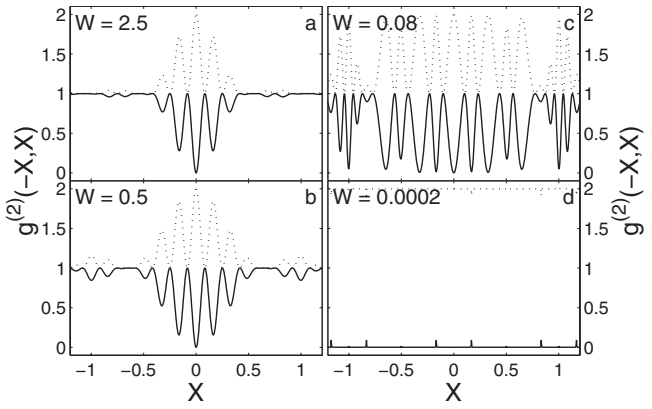

FIG. 2. Normalized second-order correlation functions $g^{(2)}(-X,X)$ corresponding to Fig. 1. Solid lines and dashed lines are for the fermion source and the boson source, respectively.

that the second-order interference can exhibit both wave and particle natures. The interference reflects the wave nature, while the bunching or antibunching effect in two-particle interference basically can be regarded as the particle nature. In the second-order correlation the near-degenerate particles contribute to the constructive interference, resulting in the maximum for bosons and the minimum for fermions due to the Pauli exclusion principle. As the bandwidth is decreased, e.g., $W=0.5$, the intensity distribution [the first term of the right part in Eq. (6b)] exhibits the bright fringe, and the second-order interference fringe for fermions varies from dark to "half bright" in Fig. 1(b). Furthermore, in the narrow bandwidth limit, both the terms of the right part in Eq. (6b) are closer to $\tilde{D}^2(kx/z)$. As a result, their sum (for bosons) gives the fringe as the first-order one, while their difference (for fermions) keeps the subwavelength feature [see Figs. 1(h) and 1(d)]. We now survey this effect by evaluating the normalized correlation function $g^{(2)}(-X,X)=G^{(2)}(-X,X)/[G^{(1)}(-X,-X)G^{(1)}(X,X)]$, as shown in Fig. 2. We can see explicit bunching and antibunching feature in the interference: the bright fringes for bosons (dashed lines) and the dark fringes for fermions (solid lines). When the bandwidth is very small such as $W=0.0002$ in Fig. 2(d), it has $g^{(2)}(-X,X)\approx 0$ for fermions and $g^{(2)}(-X,X)\approx 2$ for bosons, verifying that the two terms of the right part in Eq. (6b) are equal.

IV. DARK GHOST IMAGING

Ghost imaging, as one of the most important aspects in quantum imaging, manifests prominent spatial correlation feature. In ghost imaging for thermal light [7,8,10,26–29], a source beam is divided into two parts: one illuminates an object (the test beam) and the other travels freely (the reference beam). Though the intensity of each beam is homogeneously distributed, the coherent information of the object can be extracted through the intensity correlation measurement of the two beams in such a way that the spatial resolution measurement is performed in the reference beam rather than in the test beam. By analyzing different correlation features between entangled photon pairs and thermal light, in Ref. [26], Cao *et al.* first pointed out that thermal light can perform ghost imaging without using any lenses. The lensless ghost imaging effect was later demonstrated experimentally [27–29]. Lensless imaging is phase insensitive and occurs at near field, i.e., the distance from source to image to be detected is the same as that from source to object. However, the far-field diffraction pattern of an object may contain its complete information including both amplitude and phase modulations. Bache *et al.* [30] observed experimentally correlated imaging of a pure phase object with a pseudothermal light source. This technique is of particular significance for microscopy using massive particle sources, such as electron microscopy, since these sources are incoherent.

In ghost imaging using a particle source, the flux of particles is divided into two parts by a beamsplitter, for example, diffraction from thin crystal lamellae offers a good beam splitting mechanism for electrons [31]. One flux penetrates through an object, described by the transmission function $T(x)$, which is placed at distances z_2 and z_3 from the source and the detection plane in the test arm, respectively. The other flux travels freely a distance of z_1 before arriving at the detector in the reference arm. In the paraxial approximation, the impulse response functions for the reference and test arms are written as

$$\tilde{h}_1(x_1,-q)=\frac{1}{\sqrt{2\pi}}\exp\left[i\left(kz_1+qx_1-\frac{z_1q^2}{2k}\right)\right], \quad (14a)$$

$$\tilde{h}_2(x_2,-q)=\sqrt{\frac{k}{2\pi i z_3}}\exp\left[i\left(kz_2+kz_3-\frac{z_2q^2}{2k}+\frac{kx_2^2}{2z_3}\right)\right] \times\frac{1}{\sqrt{2\pi}}\int T(x)\exp\left[-i\left(k\frac{x_2}{z_3}-q\right)x+i\frac{kx^2}{2z_3}\right]dx, \quad (14b)$$

respectively.

We first consider the broadband limit, $\langle n_q\rangle\to\langle n\rangle/w$, for which the analytical solutions can be acquired. Using Eqs. (7a) and (14), we obtain $G_{11}^{(1)}(x_1,x_1)=\langle n\rangle/(2\pi)$ and $G_{22}^{(1)}(x_2=0,x_2=0)=\frac{k\langle n\rangle}{2\pi z_3 w}\int dx|T(x)|^2$. Thus the first term in Eq. (7b) contributes a constant background independent of x_1. However, the first-order cross-correlation function is obtained as

$$|G_{12}^{(1)}(x_1,0)|^2=\frac{k\langle n\rangle^2}{8\pi^3 z_3 w^2}\left|\int\int dqdx \times\exp\left[i\frac{(z_1-z_2)q^2}{2k}-iq(x_1-x)\right]T(x) \times\exp\left[i\frac{kx^2}{2z_3}\right]\right|^2. \quad (15)$$

If $z_1=z_2$, Eq. (15) is reduced to

$$|G_{12}^{(1)}(x_1,0)|^2 = \frac{k\langle n\rangle^2}{2\pi z_3 w^2}|T(x_1)|^2, \tag{16}$$

where lensless ghost imaging occurs for an amplitude object. Otherwise, Eq. (15) becomes

$$|G_{12}^{(1)}(x_1,0)|^2 = \frac{k^2\langle n\rangle^2}{4\pi^2 z_3|z_1-z_2|w^2}\left|\int T(x) \times \exp\left[-ik\frac{x_1 x}{z_2-z_1} - i\frac{kx^2}{2z_{eff}}\right]dx\right|^2, \tag{17}$$

where the effective diffraction length is defined as $z_{eff}=z_3(z_1-z_2)/(z_3+z_2-z_1)$. If the two detectors have the same distances from the source, $z_1=z_2+z_3$, the quadratic phase factor in the integration disappears, and we obtain

$$|G_{12}^{(1)}(x_1,0)|^2 = \frac{k^2\langle n\rangle^2}{2\pi z_3^2 w^2}\left|\tilde{T}\left(-\frac{kx_1}{z_3}\right)\right|^2, \tag{18}$$

where $\tilde{T}(q)$ is the Fourier transform of $T(x)$. Using the effective diffraction length z_{eff}, we may define the effective Fresnel number $F_{eff}=R^2/(\lambda z_{eff})$, where R is the size of the object. When $F_{eff}\ll 1$, the quadratic phase factor can be neglected and the Fraunhofer diffraction pattern appears in the intensity correlation measurement. However, the Fresnel number in the test arm $F=R^2/(\lambda z_3)$ could be very different from F_{eff} so the interference pattern in ghost imaging will not be the same as that for coherent imaging in the test arm.

For the general spectral distribution [Eq. (10)], the analytical solutions are unavailable. Then we calculate the normalized second-order correlation function $g^{(2)}(x_1,0)=G_{12}^{(2)}(x_1,0)/[G_{11}^{(1)}(x_1,x_1)G_{22}^{(1)}(0,0)]$ numerically. As an example for fermions, we consider an electron imaging system, where the source consists of nonrelativistic electrons of energy 1 keV, corresponding to the wavelength $\lambda=0.0388$ nm. The object to be imaged is a double slit with $b=0.6$ μm and $d=1.8$ μm. The divergence angle of the electron beam 2α is assumed to be 10^{-3} rad. It follows that the transverse coherence length can be obtained by $l_s=\lambda/(2\alpha)=3.88\times 10^{-2}$ μm [32], and the normalized spectral bandwidth of the electron source is thus $W=wb/(2\pi)=b/(2\pi l_s)\approx 2.5$. Since the transverse coherent length is much smaller than the size of the double slit, the interference will not occur in the intensity measurement. In the above ghost imaging scheme, we set $z_2=50$ mm and $z_3=50$ mm and present $g^{(2)}(X_1,0)$ versus the normalized position $X_1=x_1kb/(2\pi z_3)$ in Fig. 3. We can see that, for the fermions, the images are the dark patterns against bright background. As z_1 is changed from 100 mm ($z_1=z_2+z_3$) to 50 mm ($z_1=z_2$), the patterns in the intensity correlation measurements exhibit the conversion from the Fraunhofer diffraction pattern [Fig. 3(a)], through the Fresnel diffraction pattern [Fig. 3(b)], and finally to the image [Fig. 3(d)] of the double slit, in agreement with the analytical result in the broadband limit.

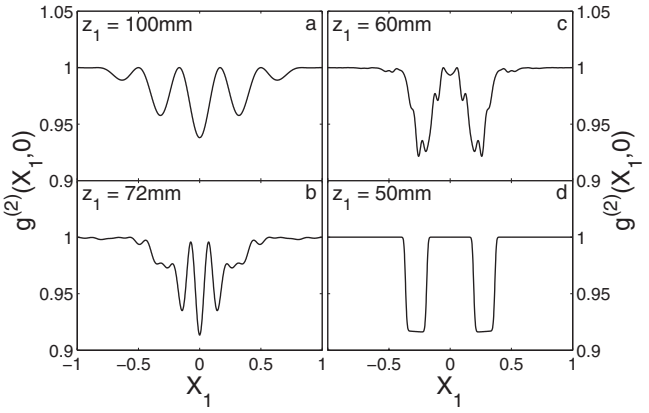

FIG. 3. Normalized second-order correlation functions $g^{(2)}(X_1,0)$ in ghost imaging of a double-slit using a thermal electron source. $X_1=x_1kb/(2\pi z_3)$ is the normalized position in the detection plane. The normalized bandwidth of the source is taken as $W=2.5$.

V. ELECTRON MICROSCOPY USING GHOST IMAGING

In traditional transmission electron microscope (TEM), an object of transmission function $T(x)$ is placed close to the front-focal plane of the objective lens, and its Fourier diffraction power spectrum $|\tilde{T}(kx_f/f_o)|^2$ can be recorded in the back-focal plane, where f_o is the focal length of the lens and x_f, the transverse coordinate in the back-focal plane [33]. The diffraction pattern can be further magnified by following lenses. To obtain the sharpest diffraction pattern, the condenser system is adjusted to illuminate the specimen with a parallel beam of electrons, satisfying better spatial coherence. For example, the beam is effectively a parallel one if its divergence angle 2α is smaller than 10^{-4} rad after collimation [34]. Both the transverse coherence length l_s and the intensity j of the beam are related to the beam divergence angle 2α as $l_s=\lambda/(2\alpha)$ and $j=\pi B\alpha^2$, respectively, where B is the beam brightness. Since B is constant in any cross section of an electron beam [32], there is a conflict between the transverse coherence length and the beam intensity. In ghost imaging, however, the transverse coherence length of the beam can be arbitrarily small so the conflict can be avoided.

In the electron microscopy, electron flux can readily penetrate through specimens so the specimens are regarded as essentially phase objects [35]. Ghost imaging for a phase object has been studied in Refs. [30,36,37], in which the diffraction pattern of the phase object is recorded. For a practical electron microscope, the diffraction pattern must be further magnified by a lens system. In the following, we propose an electron microscope sketched in Fig. 4 and discuss its feasibility. In the traditional TEM, the Fourier spatial-frequency spectrum of an object is performed through an objective lens. However, the objective lens can be saved in the present scheme, as long as $z_1=z_2+z_3$ is satisfied. In fact, the lens in Fig. 4 plays the role of magnifying the diffraction pattern. Let U and V be the object and image distances of the magnifying lens, respectively. For an ideal lens, the impulse response function from the object plane to the imaging one is given by

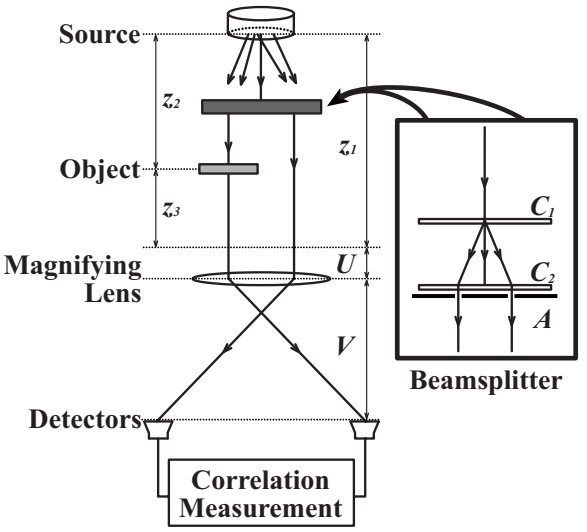

FIG. 4. Scheme of transmission electron microscope using ghost imaging. A possible beamsplitting device is sketched in the inset, where incident beam can be split by two crystal foils C_1 and C_2 through Bragg reflection, and aperture A picks out two outgoing beams.

$$h_m(x_m,x_o) = \sqrt{\frac{U}{V}}\exp\left[ik\left(U+V+\frac{x_o^2}{2U}+\frac{x_m^2}{2V}\right)-i\frac{\pi}{2}\right] \times \delta\left(x_o+\frac{U}{V}x_m\right), \tag{19}$$

where x_o and x_m are the transverse coordinates in the object and imaging planes, respectively. As shown in Fig. 4, both the reference and test beams share the same lens. Taking into account the impulse response functions of the two arms in Eq. (14), we obtain the two new ones from the source to the detection plane

$$\tilde{h}_r(x_1,-q) = \frac{1}{\sqrt{2\pi}}\sqrt{\frac{U}{V}}\exp\left[-i\frac{\pi}{2}+ik\left(U+V+z_1+\frac{U+V}{2V^2}x_1^2\right) - i\frac{U}{V}qx_1 - i\frac{q^2z_1}{2k}\right], \tag{20a}$$

$$\tilde{h}_t(x_2,-q) = \frac{1}{2\pi}\sqrt{\frac{kU}{z_3V}} \times\exp\left[-i\frac{3\pi}{4}+ik\left(z_2+z_3+U+V + \frac{z_3(U+V)+U^2}{2z_3V^2}x_2^2\right)-i\frac{q^2z_2}{2k}\right] \times\int T(x)\exp\left[i\frac{kx^2}{2z_3}+i\frac{kUxx_2}{z_3V}+iqx\right]dx. \tag{20b}$$

In the broadband limit, we obtain $G_{11}^{(1)}(x_1,x_1)=\langle n\rangle/(2\pi M)$ and $G_{22}^{(1)}(x_2=0,x_2=0)=(k\langle n\rangle/2\pi z_3wM)\int dx|T(x)|^2$, where $M=V/U$ represents the magnification. Hence the intensity distributions of the two beams are homogeneous. The first-order cross-correlation function is

$$|G_{12}^{(1)}(x_1,0)|^2 = \frac{k^2\langle n\rangle^2}{2\pi z_3^2w^2M^2}\left|\tilde{T}\left(\frac{kx_1}{Mz_3}\right)\right|^2, \tag{21}$$

where $z_1=z_2+z_3$ is used. In comparison with Eq. (18) the size of the diffraction pattern is magnified by M times.

As an example, we consider a phase double-slit as the object, whose transmission function is given by

$$T_{ph}(x) = \begin{cases} \exp(i\pi), & x\in\left[-\dfrac{d+b}{2},-\dfrac{d-b}{2}\right],\left[\dfrac{d-b}{2},\dfrac{d+b}{2}\right] \\ 1, & x\in\left(-\dfrac{d-b}{2},\dfrac{d-b}{2}\right) \\ 0, & \text{others}. \end{cases} \tag{22}$$

The Fourier transform of the phase double slit is written as

$$\tilde{T}_{ph}(q) = 1/\sqrt{2\pi}\{(d-b)\mathrm{sinc}[(d-b)q/2] + 2b\exp(i\pi)\mathrm{sinc}[bq/2]\cos(dq/2)\}. \tag{23}$$

When $d=3b$, one obtains $\tilde{T}_{ph}(0)=0$. Unlike the interference fringe of an amplitude double slit, the interference minimum appears at the symmetric center of the pattern. Hence we take $b=0.6$ μm and $d=1.8$ μm for the phase double slit in the numerical simulation.

For the general spectral distribution [Eq. (10)], we calculate the normalized second-order correlation function $g^{(2)}(X_1,0)$ for different spectral bandwidths and plot them in Fig. 5, in which we take $\lambda=0.0388$ nm, $z_1=100$ mm, $z_2=50$ mm, $z_3=50$ mm, and the magnification of the lens system $M=1000$. As indicated above, the normalized spectral bandwidth $W=2.5$ in Fig. 5(a) corresponds to the beam divergence angle $2\alpha\simeq10^{-3}$ rad, much larger than that in the traditional TEM. Figure 5(a) shows the Fraunhofer diffrac-

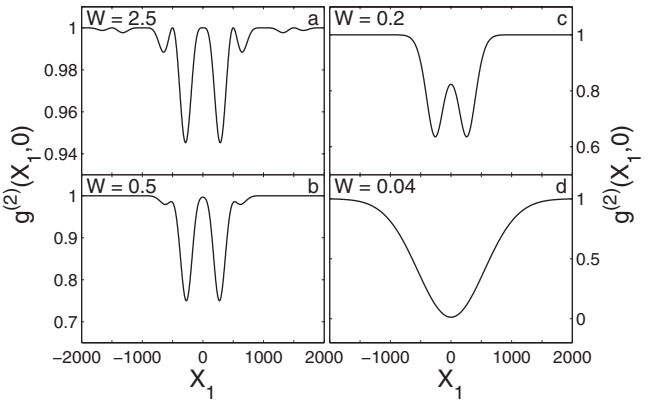

FIG. 5. Normalized second-order correlation functions $g^{(2)}(X_1,0)$ in the ghost imaging scheme of Fig. 4 for a phase double slit. W is the normalized spectral bandwidth of the thermal electron source, and $X_1=x_1kb/(2\pi z_3)$ is the normalized position in the detection plane.

tion pattern of the phase double slit, in a good agreement with Eq. (23), where $q=2\pi X_1/(Mb)$. As expected, the diffraction pattern is upside down with respect to that for thermal light. The spacing of the two minima is $\Delta X_1=500$, corresponding to a magnified spacing $\Delta x_1=Mz_3\lambda/(2b)\simeq 1.6\times 10^{-3}$ m in the real coordinate. As the bandwidth is decreased, the diffraction fringes degrade gradually. In Fig. 5(d), where $W=0.04$ corresponds to $2\alpha\simeq 1.6\times 10^{-5}$ rad and $l_s\simeq 2.4$ μm, the coherent length of the source l_s is about the same order as the object size, that is, the object is illuminated coherently. As a result, the two beams in the scheme are not correlated and the correlated diffraction fringe disappears.

VI. DISCUSSION AND CONCLUSION

The theoretical discussion above is concentrated on the spatial aspect of quantum imaging by neglecting the effect of temporal correlation and detection system. We have shown that, in this ideal case, the maximum visibility of quantum imaging for thermal fermions is 100% while it is 33.3% for thermal bosons. It is worth noting that it has taken nearly 50 years from the original HBT experiment [11] to the recent anticorrelation experiment for free electron [18]. One of the technical barriers to experimentally observing HBT effect for fermions comes from their very short coherence time. For example, the coherence time T_c for free electron is of the order of 10^{-14} s in the experiment of Ref. [18]. The time resolution T_r of the fastest detectors available are about a thousand times greater than T_c. This will greatly decrease the visibility of quantum imaging. Under the assumption of cross-spectral purity, the average rate of coincidence counter can be obtained as [20,38]

$$\mathcal{R}_c \propto 1 \pm (T_c/T_r)|g^{(1)}(x_1,x_2)|^2, \quad (T_c \ll T_r), \tag{24}$$

where the normalized first-order correlation function is $g^{(1)}(x_1,x_2)=G^{(1)}(x_1,x_2)/\sqrt{G^{(1)}(x_1,x_1)G^{(1)}(x_2,x_2)}$. Accordingly, the visibility of quantum imaging decreases about T_c/T_r.

The average occupation number of particles in the same quantum state, $\langle n_{\mathbf{k}}\rangle$, which is also called the degeneracy, plays an important role in particle correlation experiments [38,39]. It is clear that $\langle n_{\mathbf{k}}\rangle \leq 1$ for fermions. Mandel and Wolf [20] arrived that the normalized fluctuation correlation registered by two detectors is proportional to the beam degeneracy when it is low. For a realistic fermionic source the degeneracy is very low so that the observation of anticorrelation signal is difficult. The degeneracy is proportional to the source brightness [38,39]. With the advance of high-brightness field electron sources in recent years, the experimental observation of anticorrelation of free electrons becomes feasible. Likewise, the way to realize dark quantum imaging is opening.

In summary, we have shown that fermions and bosons behave the same phenomena in the first-order spatial interference and the different ones in the second-order spatial interference. As one-particle effect, the first-order interference reflects mainly the wave nature. However, the quantum statistical property of particles has been involved in the second-order interference. The antibunching effect and Pauli exclusion of fermions make coherent information in the second-order field correlation embedded in the intensity background, resulting in dark image. In this sense, quantum imaging for fermions is particularly interesting to manifest both wave and particle nature simultaneously. Furthermore, quantum imaging of massive particles is valuable since their coherent sources are unavailable. In light of this, we proposed a magnifying ghost imaging for electron microscopy, which can release the requirement of coherence in the traditional TEM.

ACKNOWLEDGMENTS

This work was supported by the National Fundamental Research Program of China, Project No. 2006CB921404, and the National Natural Science Foundation of China, Project No. 10874019.

[1] See, for example, A. Gatti, E. Brambilla, and L. A. Lugiato, in *Progress in Optics*, edited by E. Wolf (Elsevier/North-Holland, Amsterdam, 2008), Vol. 51, p. 251, and the references cited there.
[2] D. N. Klyshko, Sov. Phys. JETP **67**, 1131 (1988); D. N. Klyshko, *Photons and Nonlinear Optics* (Gordon and Breach Science, New York, 1988).
[3] T. B. Pittman, Y. H. Shih, D. V. Strekalov, and A. V. Sergienko, Phys. Rev. A **52**, R3429 (1995); D. V. Strekalov, A. V. Sergienko, D. N. Klyshko, and Y. H. Shih, Phys. Rev. Lett. **74**, 3600 (1995).
[4] E. J. S. Fonseca, C. H. Monken, and S. Pádua, Phys. Rev. Lett. **82**, 2868 (1999).
[5] M. D'Angelo, M. V. Chekhova, and Y. Shih, Phys. Rev. Lett. **87**, 013602 (2001).
[6] R. S. Bennink, S. J. Bentley, and R. W. Boyd, Phys. Rev. Lett. **89**, 113601 (2002); R. S. Bennink, S. J. Bentley, R. W. Boyd, and J. C. Howell, *ibid.* **92**, 033601 (2004).
[7] A. Gatti, E. Brambilla, M. Bache, and L. A. Lugiato, Phys. Rev. A **70**, 013802 (2004); Phys. Rev. Lett. **93**, 093602 (2004).
[8] J. Cheng and S. Han, Phys. Rev. Lett. **92**, 093903 (2004).
[9] K. Wang and D. Z. Cao, Phys. Rev. A **70**, 041801(R) (2004).
[10] Y. Cai and S. Y. Zhu, Opt. Lett. **29**, 2716 (2004).
[11] R. Hanbury Brown and R. Q. Twiss, Nature (London) **178**, 1046 (1956); **178**, 1447 (1956).
[12] G. Scarcelli, V. Berardi, and Y. Shih, Phys. Rev. Lett. **96**, 063602 (2006).
[13] A. Gatti, M. Bondani, L. A. Lugiato, M. G. A. Paris, and C. Fabre, Phys. Rev. Lett. **98**, 039301 (2007).
[14] C. Jönsson, Z. Phys. **161**, 454 (1961); Am. J. Phys. **42**, 4 (1974).
[15] R. C. Liu, B. Odom, Y. Yamamoto, and S. Tarucha, Nature (London) **391**, 263 (1998).

[16] M. Henny, S. Oberholzer, C. Strunk, T. Heinzel, K. Ensslin, M. Holland, and C. Schönenberger, Science **284**, 296 (1999).
[17] W. D. Oliver, J. Kim, R. C. Liu, and Y. Yamamoto, Science **284**, 299 (1999).
[18] H. Kiesel, A. Renz, and F. Hasselbach, Nature (London) **418**, 392 (2002).
[19] T. Jeltes *et al.*, Nature (London) **445**, 402 (2007).
[20] L. Mandel and E. Wolf, *Optical Coherence and Quantum Optics* (Cambridge University Press, Cambridge, 1995).
[21] T. Tyc, Phys. Rev. E **62**, 4221 (2000).
[22] M. P. Silverman, Nuovo Cimento B **97**, 200 (1987).
[23] T. Tyc, Phys. Rev. A **58**, 4967 (1998).
[24] J. Xiong, D. Z. Cao, F. Huang, H. G. Li, X. J. Sun, and K. Wang, Phys. Rev. Lett. **94**, 173601 (2005).
[25] G. Scarcelli, A. Valencia, and Y. Shih, Europhys. Lett. **68**, 618 (2004).
[26] D. Z. Cao, J. Xiong, and K. Wang, Phys. Rev. A **71**, 013801 (2005).
[27] G. Scarcelli, V. Berardi, and Y. Shih, Appl. Phys. Lett. **88**, 061106 (2006).
[28] L. Basano and P. Ottonello, Appl. Phys. Lett. **89**, 091109 (2006).
[29] X. H. Chen, Q. Liu, K. H. Luo, and L. A. Wu, Opt. Lett. **34**, 695 (2009).
[30] M. Bache, D. Magatti, F. Ferri, A. Gatti, E. Brambilla, and L. A. Lugiato, Phys. Rev. A **73**, 053802 (2006).
[31] L. Marton, Phys. Rev. **85**, 1057 (1952).
[32] A. Tonomura, *Electron Holography* (Springer, Berlin, 1999).
[33] J. C. H. Spence, *High-Resolution Electron Microscopy* (Oxford University Press, Oxford, New York, 2003).
[34] D. B. Williams and C. B. Carter, *Transmission Electron Microscopy* (Plenum, New York, 1996).
[35] J. M. Cowley, *Diffraction Physics* (Elsevier/North-Holland, Amsterdam, 1995).
[36] A. F. Abouraddy, P. R. Stone, A. V. Sergienko, B. E. A. Saleh, and M. C. Teich, Phys. Rev. Lett. **93**, 213903 (2004).
[37] M. Zhang, Q. Wei, X. Shen, Y. Liu, H. Liu, J. Cheng, and S. Han, Phys. Rev. A **75**, 021803(R) (2007).
[38] M. P. Silverman, Phys. Lett. A **120**, 442 (1987).
[39] T. Kodama, N. Osakabe, J. Endo, A. Tonomura, K. Ohbayashi, T. Urakami, S. Ohsuka, H. Tsuchiya, Y. Tsuchiya, and Y. Uchikawa, Phys. Rev. A **57**, 2781 (1998).